Optical diffuse reflectance accessory for measurements of skin tissue by near-infrared spectroscopy

R. Marbach and H. M. Heise

An optimized accessory for measuring the diffuse reflectance spectra of human skin tissue in the near-infrared spectral range is presented. The device includes an on-axis ellipsoidal collecting mirror with efficient illumination optics for small sampling areas of bulky body specimens. The optical design is supported by the results of a Monte Carlo simulation study of the reflectance characteristics of skin tissue. Because the results evolved from efforts to measure blood glucose noninvasively, the main emphasis is placed on the long-wavelength near-infrared range where sufficient penetration depth for radiation into tissue is still available. The accessory is applied for *in vivo* diffuse reflectance measurements.

Key words: Diffuse reflectance accessory, near-infrared spectroscopy, human tissue, near-infrared optical parameters of skin, Monte Carlo simulation, radiation transport.

1. Introduction

As a result of technical progress and increasing demands for medical treatment and diagnostic methods that are gentle, the use of optical spectroscopy in the field of biomedical applications has been rapidly increasing. Different biological effects, e.g., of heating tissue by intense laser sources, are in use for a variety of medical treatments.[1] Generally the wavelengths are chosen to be within the therapeutic window between 600 and 1300 nm in which the greatest penetration depth into tissue is available.[2] To obtain quantitative information about various analytes in tissue or blood, optical diagnostic techniques usually measure a broad spectral range, permitting multivariate calibration modeling, which is preferred to univariate regression because of inherently improved accuracy, precision, and reliability. An important example is the noninvasive, i.e., transcutaneous determination of blood oxygenation by near-infrared (NIR) spectroscopy (see Ref. 3) currently accepted for clinical use. An even more demanding goal is the measurement of oxygen saturation of cerebral blood by transillumination of the heads of newborn infants,[4] an apparatus for the *in vivo* monitoring of the oxygenation of blood and brain tissue stems from this research.

From a medical point of view, an important blood analyte to be determined by a noninvasive technique is blood glucose. Such a device significantly improves self-monitoring, especially for insulin-dependent patients suffering from diabetes mellitus. Replacing today's invasive devices for determining blood glucose concentration with a transcutaneously measuring apparatus would allow for more frequent measurements, eventually providing a virtually closed-loop control system. Unfortunately the quantitative analysis of tissue-absorbance signals for glucose is very demanding and ambitious, because the glucose concentration is rather low ($\sim 0.1\%$ in blood) and the absorbance signals are weak as well as being overlapped by a varying, dominant background signal.

Because of the promising results of calibration experiments for glucose in human plasma samples measured by NIR spectroscopy,[5,6] we investigated the potential of this spectral range for a noninvasive measurement, the results of which are published elsewhere.[7] Our emphasis was mainly focused on the wavelength range near 1.6 μm where glucose absorptivities of acceptable magnitude exist. The inner lip promised the best opportunities for a trans-

When this research was performed, the authors were with the Institut für Spektrochemie und angewandte Spektroskopie, Bunsen-Kirchhoff-Strasse 11, D-44139 Dortmund, Germany. R. Marbach is now with Biocontrol Technology, Inc., 300 Indian Springs Road, Indiana, Pennsylvania 15701.

Received 24 August 1993; revised manuscript received 15 June 1994.

0003-6935/95/040610-12$06.00/0.

cutaneous glucose measurement, because it is a rather homogeneous tissue rich in capillary blood vessels. Kaiser[8] has proposed a noninvasive blood glucose assay by mid-IR spectrometry, using the attenuated total reflection (ATR) technique. In a paper published recently Kajiwara *et al.*[9] report on results from analyzing the ATR spectra of oral mucosa. We also studied this option[6] but found experimental evidence that the true correlation of blood glucose concentration to the lip spectra based on glucose absorption near $\lambda = 9.6$ μm could not be realized because of the minute radiation penetration depth into tissue rendered by the ATR technique.

For the NIR spectral range chosen we studied the optical behavior of skin tissue in a diffuse reflectance experiment by Monte Carlo simulations. Also of interest to us was the tissue penetration depth achievable by this technique. As a result of our investigation a throughput optimized accessory for diffuse reflectance was designed. The requirements for our application are as follows:

(1) *In situ* measurements of small spots from bulky body specimens with a minimum of inconvenience for patients.
(2) High reproducibility regarding the measurement of tissue and reference standards.
(3) Sufficient optical throughput for the optimization of the spectral signal-to-noise ratio.
(4) Rejection of specularly (Fresnel) reflected radiation.

The last requirement is important, because the Fresnel-reflected radiation from the skin, which is mainly directed into a distinct solid angle defined by the macroscopic surface normal of the sample, can reach the same order of magnitude as the diffusely reflected fraction from the inside tissue that bears the information necessary for a noninvasive assay. For a perpendicular incidence, for example, the reflectance at an interface with a pair of refractive indices of $n_1 = 1.0$ and $n_2 = 1.4$ is 2.8%. The constructed accessory makes provision for the exclusion of this part, which renders complications for the intended quantitative spectrometric analysis. Results from *in vivo* diffuse reflectance measurements with this accessory are reported and compared with those from Monte Carlo simulations.

2. Optical Design

Diffuse reflectance spectroscopy is a widely applied technique in the IR spectral range, so that a variety of accessories for this purpose have been designed. There are optical devices for the measurement of the absolute reflectivity with integrating spheres (see, for example, Refs. 10–12); however, for the analytical applications, as in particular quantitative spectrometric analysis of samples from the agricultural and food industry, relative measurements suffice. There is another category based on ellipsoidal segmented mirrors that are commercially available and placed conventionally in the spectrometer sample chamber. Based on the symmetric design, half of the entire hemisphere above the sample is considered for illumination and the collection of the diffusely reflected radiation, although to reject the Fresnel-reflected radiation a smaller solid angle is available (for a recent application see, for example, Ref. 13). Generally only small-sized samples can be investigated except in an alternative design (an upward looking praying mantis) by which spots on bulky samples such as films can also be studied. The design of several accessories was recently reviewed.[14]

Another category includes devices with dedicated detectors, which are usually attached to a spectrometer. For these devices the adaptation of the field of view of commercially available detectors is a general design problem. In particular, for liquid-nitrogen-cooled semiconductive detectors a field of view of 60° is standard. A possible adaptation to the limited solid angle is offered by the design of Dunn *et al.*[15] (see also Refs. 16 and 17), by which, however, only small-sized samples can be studied. This hindrance does not exist for the configuration proposed by Korte,[18] which permits bulky samples to be studied. The realization of such a design with a so-called light pipe for illumination has been described.[14,19] Because of the considerably low transmittance of the light pipe chosen, only 1% of the radiation compared with the energy in the sample chamber focus reaches the detector when a white Lambertian scattering material is measured.

To suppress the Fresnel-reflected radiation, it is advantageous to irradiate the sample by a converging beam with a half-angle α_0 around the macroscopic surface normal, so that the specularly reflected radiation, dependent on the sample roughness, can be found preferably within the solid angle $\Omega_0 = 2\pi(1 - \cos \alpha_0)$ used for illumination. The optical conductance of such a beam that produces a circular focus with an area of πr_0^2 is well approximated by $G_0 = \pi^2 r_0^2 \sin^2 \alpha_0$. The optical conductance is an invariant for the optical beam within a well-designed spectrometer. One can approximate it, taking the integral over the actual solid angle Ω, by $G = A \int \cos \alpha \, d\Omega$, where A is, e.g., the area of any source image, α is the angle of a given ray with respect to the normal of that area, provided its dimensions are small in relation to the distance from the next optical element (see also Ref. 18 and the literature cited therein).

The principal problem for the construction of a diffuse reflectance accessory is that the law of invariance of the optical conductance is not valid throughout, because the reflected radiant power is distributed over the total hemisphere above the sample. Furthermore the diffusely radiating area is increased to $\pi(r_0 + r_d)^2$, where r_d describes the fringing of the illuminated spot by the photon migration within the tissue. The optical conductance of the diffusely reflected beam is $G_{\text{diff}} = \pi^2(r_0 + r_d)^2 \sin^2 \alpha_{\text{diff}}$ with $\alpha_{\text{diff}} = 90°$ being significantly greater than the optical conduc-

tance used for irradiation, which should be adapted in an optimally constructed spectrometer to that of its detector with $G_{det} = \pi^2 r_{det}^2 \sin^2 \beta_0$. A loss-free projection of G_{diff} to G_{det} is impossible, because for collection of the diffusely reflected radiant power only the annular solid angle $\Omega_c = 2\pi - \Omega_0$, with exclusion of the illumination cone, is available.

There are three different aspects to the optimization of such an accessory:

(1) The competition between the solid angle for illumination Ω_0 and collection Ω_c above the sample surface must be considered.

(2) The annular solid angle $\Omega_c = 2\pi \cos \alpha_0$ left for collection has to be projected onto a detector with a standard field of view of $2\beta_0 = 60°$.

(3) The optical elements for sample irradiation must fit into the cone with a half-angle of α_0 with minimum loss caused by vignetting from the element support.

The criteria for the selection of an optimal solid angle for irradiation have been discussed by Korte[18] and Hirschfeld[20] for mid-IR application. Because the additive detector noise depends on the square root of the detector area, the choice was based on a combination of collection efficiency and the size of the radiation focus used for detection. The optimum half-angle for illumination for samples with diffuse Lambertian reflectance characteristics was found by both authors to be $\sim \alpha_0 = 40°$.

For the NIR spectral range the signal-to-noise ratio of the spectra is limited by the photon shot noise of the signal, so that an increase in detector area is not as punishable as in the mid-IR. In principle, all radiant power from the solid angle Ω_c could be focused onto a large enough detector. However, the InSb detectors that perform well in the long-wavelength NIR range are available only to a diameter of ~ 5 mm. Thus the goal is to maximize the irradiance in the focal detection plane.

The accessory that is realized based on the recent design by Korte and Otto[14,19] is shown in Fig. 1. For the on-axis ellipsoidal mirror M1 the lengths of the axes of the generating ellipse were chosen to be at a ratio of 2:1. The actual geometry was 100 mm for the major half-axis. By presupposition of a cone angle of $\alpha_0 = 30°$ for illumination and $\beta_0 = 30°$ for half of the detector field of view, the ellipsoid M1 can be cut in its equatorial plane, which aids in construction. The distance between the equatorial and the focal plane is 86.6 mm. Such an ellipsoid was manufactured by Hanseatische Orbittechnik (Bremen, Germany) with its mirror surface gold coated.

For optimization of the half-angle α_0 the following presumptions are made:

(1) The radiant power of $P_0 = L_0 \pi^2 r_0^2 \sin^2 \alpha_0$ is focused onto the skin with the radiance L_0 independent of the position and incident angle.

(2) A fraction R_{diff} of the radiation is diffusely

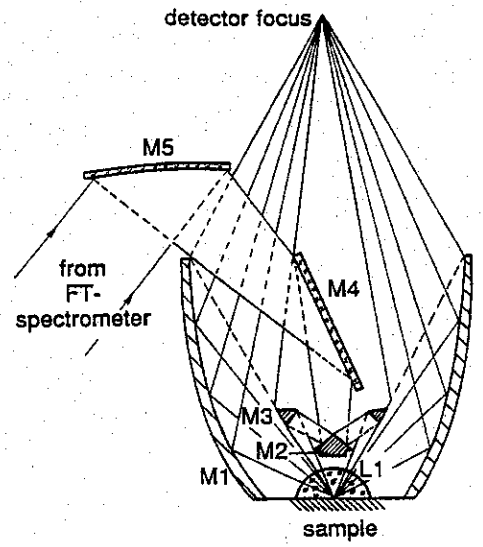

Fig. 1. Schematic of the optical accessory layout. The mirrors are as follow: M1, on-axis ellipsoid; M2/M3, axicon pair; M4, plane; M5, off-axis paraboloid; L1, immersion lens.

reflected that possesses Lambertian characteristics verified by Monte Carlo simulation as described below; the effective magnification $V_{eff}(\alpha_0) = r_{det}/(r_0 + r_d)$ produced by the ellipsoidal mirror when a Lambertian spot is imaged onto the detector can be defined, e.g., by use of the 75% quantiles of the radial distribution of the radiant power in the detector plane (see Appendix A). The analytical expressions for the α-dependent magnification of an on-axis ellipsoidal mirror were recently given by Korte.[18]

In these conditions the criterion for optimization of the irradiance in the detector focus is derived from

$$E_{det}(\alpha_0) = \frac{L_0 \pi^2 r_0^2 \sin^2(\alpha_0) R_{diff}}{\pi (r_0 + r_d)^2} \frac{[1 - \sin^2(\alpha_0)]}{V_{eff}^2(\alpha_0)}$$

$$= \frac{L_0 R_{diff}}{V_{eff}^2(\alpha_0)} \frac{\pi r_0^2}{(r_0 + r_d)^2} \sin^2(\alpha_0) \cos^2(\alpha_0) \left(\frac{W}{mm^2}\right). \quad (1)$$

The first factor in the upper row provides the radiant exitance of the diffusely radiating skin spot, and the numerator of the second term gives the collection efficiency, whereas the imaging characteristics of the ellipsoidal mirror are considered with the factor $V_{eff}(\alpha_0)$. If the photon migration in the tissue is neglected ($r_d = 0$) and the magnification is independent of α_0, the optimization criterion yields $\alpha_0 = 45°$, which is equivalent to halving the optical conductance of the hemisphere for illumination and collection. The Monte Carlo simulations in the spectral range near 1.6 μm, which is described below, estimate a value of $r_d = 0.5$ mm. The radius of the illumination focus r_0 can be steered by different apertures with radius r_{ap} chosen in the attached spectrometer, which influences the radiant power reaching from the radiation source. With the $f/4.5$ optics of the Bruker

IFS 66 spectrometer (half-angle $\alpha_{IFS} = 6.4°$), for which the accessory was intended, the parameter r_0 can be given by

$$r_0 = r_{ap} \sin \alpha_{IFS} / \sin \alpha_0, \quad (2)$$

where α_0 results from the appropriate transfer optics.

In Fig. 2 the dependence of the irradiance in the detection focus on the half-angle α_0 for illumination is exemplarily shown for different values of r_d and r_{ap} by use of the ellipsoidal configuration as given above. From Eq. (1) the optimum angle is found to shift toward a lower value than that given by Korte.[18] The calculations show that, because of photon migration, the optimum half-angle is moved further downward the larger the relative spot magnification by outfringing is (see Fig. 2, curves d and e; the difference in maximum position is 2.5° for the values used in the model calculations). We slightly altered the half-angle for illumination ($\alpha_0 = 35.3°$) because of the optical requirements for the illumination optics that is discussed below, so that a smaller solid angle for detection resulted than is provided for by the criterion of Eq. (1), which reduces the irradiance in the detector plane theoretically by ~15%. The on-axis rotational ellipsoid now collects the diffusely reflected radiation with Lambertian characteristics in the range between 90° and $\alpha_0 = 35.3°$ with an efficiency of $\eta = (1 - \sin^2 \alpha_0) = 0.67$. It must be remembered that with the mirror geometry that we chose, only beam angles with $\alpha \geq 30°$ exist for collection, because the ellipsoidal mirror M1 extends only to its equatorial plane.

Improvements in the illumination optics over the design used previously[19] were essential. The transfer optics is sketched in Fig. 3. From the Fourier-transform spectrometer the collimated beam is directed through the housing sidewall and is reflected by two plane mirrors (M6, M7) upward to a 90°

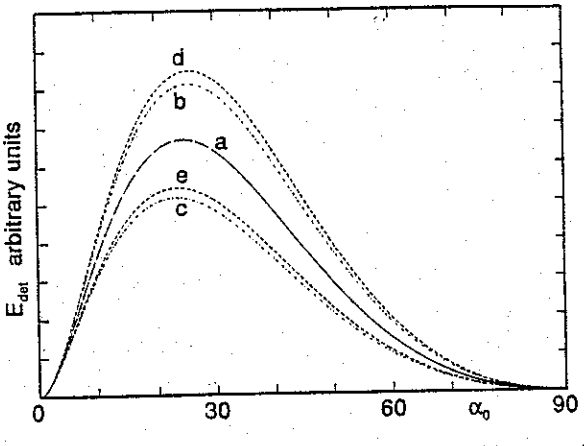

Fig. 2. Dependence of the average irradiance (in arbitrary units) in the detector plane on the half-open angle α_0 defining the illumination cone. (The effective magnification is based on the 75% quantiles of the radial distribution of the radiant power in the detector plane.) a, $r_d = 0.5$ mm, $r_{ap} = 1.5$ mm; b, $r_d = 0.5$ mm, $r_{ap} = 1.8$ mm; c, $r_d = 0.5$ mm, $r_{ap} = 1.2$ mm; d, $r_d = 0.4$ mm, $r_{ap} = 1.5$ mm; e, $r_d = 0.6$ mm, $r_{ap} = 1.5$ mm (for further details see text).

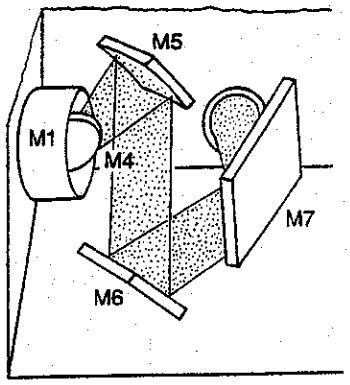

Fig. 3. Schematic of the transfer optics (for mirrors M1, M4, and M5, see also Fig. 1). Mirrors M6 and M7 are plane.

off-axis paraboloid (M5) from Bruker (Karlsruhe, Germany) with an effective focal length $f = 152.4$ mm and $f/3.81$. The paraboloidal mirror is identical to the mirror that collimates the radiation into the Michelson interferometer of the Bruker IFS 66 Fourier-transform spectrometer. It produces an image of the field-stop aperture of the spectrometer at a unit magnification of ~19 mm below the focal plane of the ellipsoidal mirror by means of plane mirror M4 intersecting the optical axis of the collecting ellipsoidal at an angle of 22.5°. The beam is further concentrated by use of a Cassegrain-similar objective M2/M3 (see Fig. 1). This pair of axicon mirrors was supplied by Spectra-Tech (Warrington, UK) and is normally used in the ATR-Circle cell.[21] Mirror M3 was reduced in size to fit into the illumination cone that we chose as discussed above. An advantage of these optics is the possibility of adjusting the half-angle for illumination by shifting the paraboidal focus produced by mirror M5 along the optical axis of the ellipsoid M1 while the Cassegrain pair is kept at a fixed position above the sampling plane, virtually without affecting the quality of the illumination focus. To realize this property, one can translate both mirrors M5 and M6 by a carriage stage parallel to the optical axis M4–M5 or M6–M7, respectively. A beam-condensing factor of ~3.7 results from the conical mirror configuration M2/M3.

A further demagnification is given by the hemispherical immersion lens (L1 in Fig. 1) made of CaF_2 with radius $r_L = 10.0$ mm from Pörschke (Höchst/Odw., Germany) and a refractive index of $n_L = 1.426$ at $\lambda = 1.6$ μm. The refractive index of CaF_2 changes only slightly within the NIR spectral range, e.g., $n_L = 1.428$ at 1.25 μm and $n_L = 1.422$ at 2.3 μm.[22] The image reduction is given by the factor[23] $n_L^{-1} = 0.7$. The influence of the lens for the collection of diffusely reflected radiation was studied with a Monte Carlo simulation for which the Fresnel losses at the spherical lens surface were considered. Absorption loss by the CaF_2 material is negligible. The results given for a circular, diffusely radiating spot with radius r_s show that the spot diameter could approach half of the lens diameter, leaving the diffusely transmitted radiation ($T = 97\%$) unchanged. The aplanatic approxima-

tion providing a linear magnification of n_L when the diffusely radiating spot is imaged through the lens is also reasonable for a Lambertian source: For $r_s \leq 0.3r_L$ only 10% of the transmitted radiation apparently starts from an annular area with r greater than $n_L r_s$. Based on its size of 10-mm diameter, the immersion lens possesses nearly aplanatic properties, because for our application r_s is smaller than $0.15r_L$. The advantages of the lens for the transcutaneous reflectance measurement of human skin lie in the fact that a refractive-index matching for skin and lens material exists (matched boundary condition), thereby suppressing the Fresnel reflection and increasing the diffuse reflectance of the tissue by a gain factor[24] of $\sim n_{\text{tissue}}^2$. Furthermore the lens allows for a reproducible presentation of the lip tissue for measurement.

The lens is mounted in a circular holder made from copper bronze with high thermal conductivity, which can be screwed into a baseplate, permitting the lens position to be aligned along the optical axis of the ellipsoidal mirror. The baseplate itself can be thermostated and carries the Cassegrainlike pair of mirrors M2/M3 by means of a tripod mount. Vignetting losses occur within the collecting mirror through the tripod (9.3%), the mount of mirror M2 through three pinholders (7.2%), and by the sidearm for the fixing mirror M4 (2.3%). Under the assumption of nearly perfect index matching between skin and the CaF_2 lens, only Fresnel reflection losses at the hemispherical lens surface of 6.2% must be taken into account. When we consider these losses a total collection efficiency of $\eta_{\text{eff}} = 0.52$ is the result, which can be realized with the InSb detector used (detector element diameter, 4 mm) for sample spots to a diameter of ~ 2 mm.

The accessory, including the transfer optics, is housed in a N_2-purgeable box and attached sideways to our spectrometer, so that easy access for *in vivo* tissue measurements is possible. Other standard applications with, for example, powders or pastes are possible by use of cups mounted in front of the lens. The spectral range to be studied with this accessory is naturally limited by the spectral transmittance of the lens material. With CaF_2, studies in the mid-IR can also be undertaken, however, with a wavelength cutoff limit of ~ 10 μm. Extension is possible with the choice of BaF_2, for example, as the lens material.

3. Monte Carlo Simulation

Our main interest was the mucous tissue of the human inner lip for several reasons. Of importance is the missing stratum corneum with the effect that the layered structure usually found for skin is less pronounced (see Fig. 4). Consequently the presupposition of an homogeneous structure used for the simulation can be accepted for an approximation. The inner lip is rich in capillary vessels in the dermis section, well thermostated, and hydrated. This section of the lip can have perfect contact with the immersion lens material used for refractive-index matching to reduce Fresnel reflection while providing

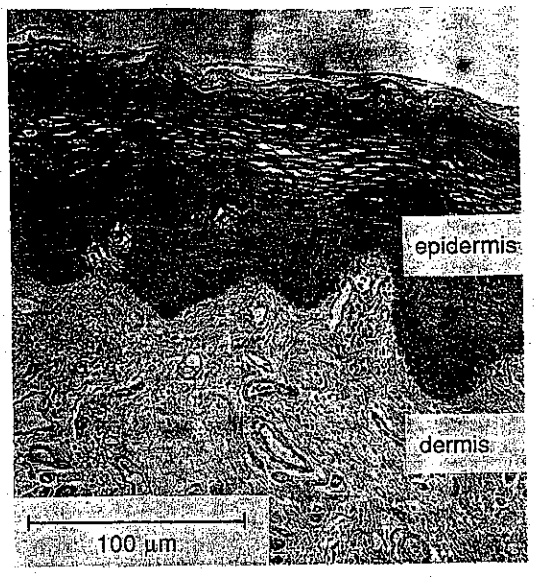

Fig. 4. Microscopic cross section of mucous lip tissue.

tolerable conditions for the patient. For insight into the radiation propagation characteristics in tissue, sample simulation studies were carried out for some of the spectral wavelengths of interest. Of concern were the average penetration depths in addition to detailed distribution functions and the spread of the reflected radiation after its propagation in tissue.

The NIR-optical properties of the tissue are considered from the viewpoint of radiative transport theory. The Monte Carlo simulation models the propagation of individual photons that are randomly scattered and absorbed in the tissue and provides us with a numerical solution of the Boltzmann transport equation (for an illustration of the random-walk process, see Fig. 5). One can evaluate the macroscopic optical characteristics by averaging the events of a great number of photons (see, for example, Refs. 25 and 26). The applicability of this theory for biological tissues in the visible and NIR spectral range is well established.[27,28] For a simulation the absorption and scattering coefficients, μ_a and μ_s, respectively, are necessary. Scattering in soft tissue is due mainly to discontinuities in the refractive index on the subcellular level. Except for striated muscle fibers (see, for example, Ref. 29) and presumably a small layer in the epidermal oral mucosa (see Fig. 4), biological tissue is optically isotropic, so that a single parameter θ, the angle of photon deflection after scattering, suffices for the description of the angular scattering intensity distribution $S(\theta)$, which is called the scattering phase function. The important parameter of $S(\theta)$ is the anisotropy parameter $g = \langle \cos \theta \rangle$ ranging from $-1 \leq g \leq 1$. In biological tissues, scattering is highly forward directed (see Fig. 5C), and the analytical expression for $S(\theta)$ is usually derived from the Henyey–Greenstein function.[30–33]

The Monte Carlo simulations were carried out for the following wavelengths: at $\lambda = 1.57$ and 2.27 μm, where absorption maxima for glucose exist, and for comparison also at $\lambda = 1.25$ μm within the therapeu-

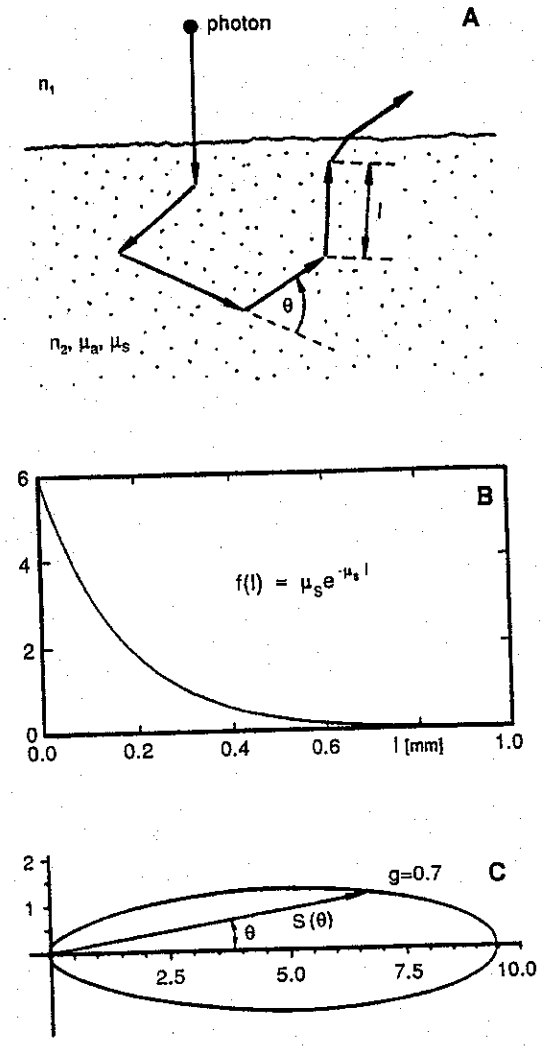

Fig. 5. Monte Carlo simulation of a diffuse reflection experiment for skin tissue: A, random walk of a single photon with scattering angle θ and random length between two scattering events l; the transparent medium above is characterized by its refractive index n_1, the optical medium below by n_2, and the absorption and scattering coefficients by μ_a and μ_s, respectively. B, probability density function of the random length between two scattering events; we take absorption into account by multiplying the weight of the photon by $\exp(-\mu_a l)$. C, scattering phase function, i.e., the probability density function of the deflection angle for a single scattering event (in polar coordinates).

tic window. A problem for the simulation is the rather scarce data on optical parameters for the spectral range of interest, because most data were published for the He–Ne laser wavelength at 633 nm.

To model the reflection at the tissue surface the refractive index is necessary. For different biological tissues[34] it was found to vary between 1.38 and 1.41 (for comparison at 630 nm, $n = 1.33$ for water[35]). A consistent result is obtained with the equation $n = 1.53–0.2w$, which depends on the water mass fraction w in tissue as proposed by Wilson and Jacques.[25] The refractive index of water decreases only slowly toward the NIR ($n = 1.32$ at $\lambda = 1.57$ μm), so for the surface tissue a value of $n_{tissue} = 1.37$ (water mass fraction assumed, $w = 0.75$) was accepted at the latter wavelength. At other wavelengths the value was adjusted according to the dispersion of water.

For a broad spectral range, including the NIR, the optical parameters μ_a, μ_s, and g were determined by Parsa *et al.*[36] for rat liver. It can be shown that the wavelength dependence of the scattering coefficient is of the order of $\lambda^{-1.4}$, which was used by us for supporting appropriate coefficients (see below). For human dermis tissue[31] the optical parameters were measured *in vitro* only at 633 nm, providing the basis for a better estimate for our case study. On the grounds of the slow functional dependence, the value found with $g = 0.8$ was transferred to our simulations. The scattering coefficients chosen are shown in Table 1.

A rather useful relationship between the optical parameters μ_a, μ_s, and g can be derived by similarity transformations of the Boltzmann transport equation. With knowledge of two parameters, we can determine the third one by measuring the diffuse reflectance of the medium, which may be used for a validation of the estimated values.[25] This method was applied for approximating the scattering coefficient; as for $\lambda = 1.57$ μm, a goniometric reflectance analysis of skin is available.[37] It is remarkable that the value obtained for the scattering coefficient follows the same wavelength dependence as that evaluated with the data from rat liver,[36] when this value is compared with the dermis parameter[31] at 633 nm. The values at the other wavelengths ($\lambda = 2.27$ and 1.25 μm) were therefore interpolated and extrapolated, respectively,

Table 1. Optical Parameters and Results for the Monte Carlo Simulation of the Diffuse Reflectance of Mucous Lip Tissue[a]

Optical Simulation Parameters[b]				r_{av} (mm)	Θ_{av} (deg)	$z_{max,av}$ (mm)	L_{av} (mm)	R_{diff} (%)
$\lambda = 1.25$ μm	$\mu_a = 0.3$	$\mu_s = 7.0$	$n_1 = n_2 = 1.37$	0.34	44.9	0.50	1.99	27.2
$\tilde{\nu} = 8000$ cm^{-1}			$n_1 = 1.0, n_2 = 1.37$	0.38	44.5	0.54	2.48	16.4
$\lambda = 1.57$ μm	$\mu_a = 0.9$	$\mu_s = 5.0$	$n_1 = n_2 = 1.37$	0.27	47.1	0.31	1.06	8.7
$\tilde{\nu} = 6350$ cm^{-1}			$n_1 = 1.0, n_2 = 1.37$	0.27	44.7	0.37	1.25	4.1
$\lambda = 2.27$ μm	$\mu_a = 1.8$	$\mu_s = 3.0$	$n_1 = n_2 = 1.34$	0.21	50.3	0.19	0.60	2.5
$\tilde{\nu} = 4400$ cm^{-1}			$n_1 = 1.0, n_2 = 1.34$	0.18	45.6	0.23	0.64	1.1

[a] R_{diff} is the total diffuse reflectance into the hemisphere above the skin (without Fresnel reflectance that must be added in unmatched boundary conditions); r_{av}, Θ_{av}, $z_{max,av}$, and L_{av} are the mean values of the radial distance to the photon exit location, the exit deflection angle, the maximum penetration depth, and the integral tissue path length, respectively.

[b] The tissue parameters μ_a and μ_s are natural logarithms based in units of mm^{-1}; n_1 is the refractive index of the medium above the skin and $n_2 = n_{tissue}$. For all simulations the anisotropy parameter was $g = 0.8$.

by means of the functional dependence found for the scattering coefficient. The parameters μ_a were chosen on the grounds that within the therapeutic window a nearly constant value can be assumed, so the dermis value at 633 nm was rounded for the wavelength at $\lambda = 1.25$ μm, which is in agreement with the results from a recent study of Maitland *et al.*[38] For the longer NIR wavelengths, the absorption coefficients of gallbladder tissue from the latter publication, which are close to those of water, were used as an approximation. The values in Table 1 are estimates of the optical parameters in the NIR, and at the moment a statement about parameter variation, e.g., resulting from biological differences, is impossible. However, this semiquantitative study based on these parameters allows for a better understanding of the *in vivo* NIR reflectance spectroscopy.

The Monte Carlo simulation was programmed with MATLAB (The Mathworks, South Natick, Mass.). For a description of comparable program codes see, for example, Refs. 39 and 40. A photon beam of infinitesimal diameter was directed perpendicularly onto the perfectly plane surface of a semi-infinite tissue sample, and a total of 10.000 diffusely reflected photons was accumulated in the hemisphere above. The attenuated exit energy of the photons was considered as a weight factor for establishing the distribution functions of interest. The history of each photon was followed to a fraction of 5×10^{-4} of its original energy. It was confirmed that this limit did not influence the simulation results.

Within the spectral range of the glucose absorption band near 1.57 μm, a transmittance of only ~0.1% for a tissue layer thickness of 3 mm results. The average pathlength through the tissue is close to the 1.4 fold of the layer thickness, which sets limitations on the transillumination of body parts such as the earlobe and web skin, e.g., between the thumb and forefinger, so that a transmittance experiment can be suggested only within the therapeutic window between 1300 and 600 nm.

In the following the results of the simulation of a diffuse reflectance experiment are described. The radial distance r (in millimeters) of the exit location with reference to the original entry spot, the exit angle Θ of the direction of photon propagation versus the surface normal, the maximum penetration depth z_{max}, and the total path length L within the tissue, the latter both in millimeters, were determined in addition to the residual energy. For the simulation either the matched boundary condition with refractive indices of $n_1 = n_2$, which can be realized by use of an appropriate immersion lens material, or a diffuse reflection into air with $n_1 = 1.0$ (see also Table 1) was considered. The average results for the parameters above and the total diffuse reflectance into the hemisphere above the skin (without the Fresnel-reflected part that must be added in unmatched boundary conditions) are summarized in Table 1. More detailed information is in Fig. 6, which shows the corresponding distribution functions.

For the matched boundary condition we must point out that the distribution functions for the direction angle Θ differ more from the Lambertian characteristic than for the unmatched case, which is also reflected by the population averages (see Table 1). The diameter of the radiating sample spot can be approximated by 1 mm. The average penetration depth is of the order necessary to reach the capillary system in the dermis part of the mucous tissue. For the matched refractive-index case the average values for penetration depth and total path length are smaller, because internal reflection at the tissue border does not exist. In addition the diffuse reflectance can be significantly increased compared with the unmatched condition as discussed in Section 2.

4. Applications

In vivo reflectance spectra that demonstrate the spectroscopic potential of the accessory constructed are shown below. For the measurements a nitrogen-cooled InSb detector (element diameter size, 4 mm) from Infrared Associates (Suffolk, UK) was installed. The Fourier-transform spectrometer (Model IFS 66) from Bruker (Karlsruhe, Germany) was equipped with a CaF_2 beam splitter and tungsten lamp. The spectral resolution chosen was usually 32 cm^{-1}. We recorded the spectra by averaging 1200 single-sided interferograms that were apodized by a Blackman-Harris three-term function. The measurement time was 1.2 min for a single-beam spectrum. The reflectance spectra are calculated from the quotient of two single-beam spectra, $\phi_s(\tilde{\nu})$ and $\phi_0(\tilde{\nu})$, either with tissue or a reflectance standard, respectively. The spectral radiant energy flux $\phi(\tilde{\nu})$ for the corresponding spectra is characterized by the spectral radiance

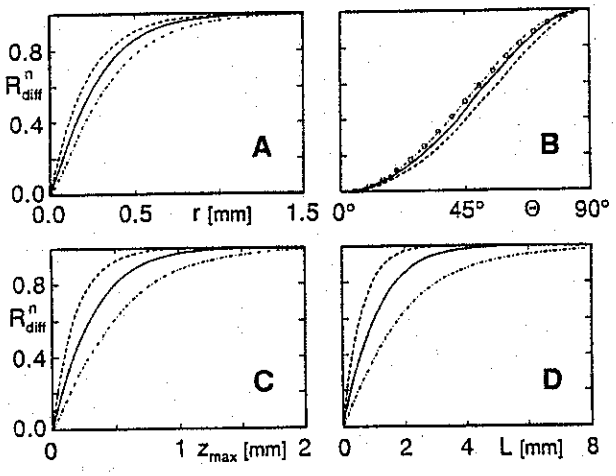

Fig. 6. Monte Carlo simulation results for a diffuse reflection experiment with mucous lip tissue: Cumulative distribution functions of the normalized diffuse reflectance for matched boundaries at $\lambda = 1.57$ μm (solid curves), $\lambda = 2.27$ μm (dashed curves), and $\lambda = 1.25$ μm (dashed–dotted curves) versus A, the radial distance of the tissue exit location; B, the exit deflection angle Θ measured against the skin normal (the trace with O gives the ideal Lambertian characteristic); C, the maximum penetration depth z_{max}; and D, the integral tissue path length of the reflected photons.

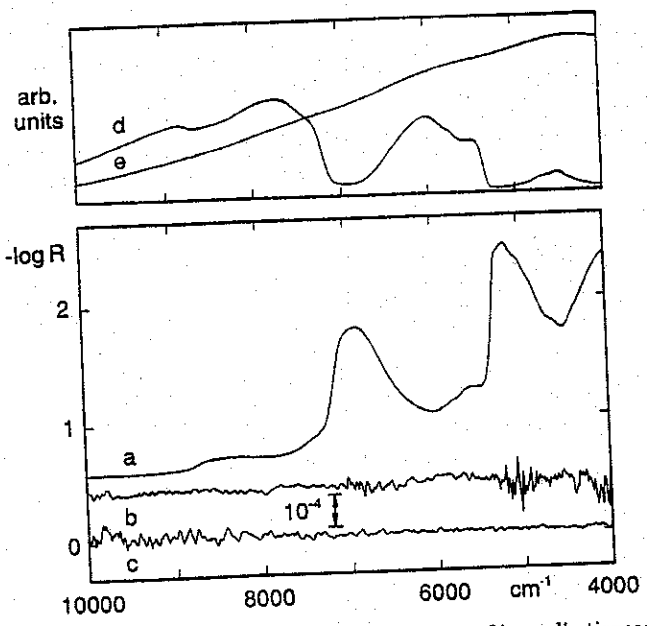

Fig. 7. *In vivo* diffuse reflectance spectroscopy of inner lip tissue: a, $-\log R$ spectrum from a test on a male person as calculated with a white Spectralon reflection standard; b, c, $-\log R$ noise level obtained from two consecutive spectra of lip tissue and a gray standard with reflectivity of ~0.1, as considered for the *in vivo* measurements (enlarged and shown with offset for clarity; the enclosed scale is for both traces); d, e, the corresponding single-beam spectra as provided for traces b and c.

of the source and other inherent characteristics from the detector, optical components, and the sample.

Spectralon distributed by Labsphere (North Sutton, N.H.) can be used as a standard material suitable for reference measurement in the visible and NIR spectral ranges, providing nearly ideal diffuse Lambertian reflectance characteristics. Advantages of this material compared with other standards such as potassium bromide powder or diffusely reflecting gold coatings (used generally for mid-IR applications) are its ease in mechanically processing, its robustness against environmental effects, such as humidity, and its efficiency for surface cleaning. In the 0.4–1.6-μm interval, the rather constant reflectivity of the white standard (SRM-99L-100C) is better than 0.98, and for longer wavelengths it decreases slightly ($R_{\lambda=1.8\,\mu m}$ = 0.976, $R_{\lambda=2.0\,\mu m}$ = 0.957, and $R_{\lambda=2.2\,\mu m}$ = 0.944).[41] For the lip reflectance measurements gray Spectralon materials possessing reflectivity values between 8% and 15% were used, so that we could consider a greater radiant power without saturating the detector signal or the ancillary amplification and digitization electronics.

Table 2. Comparison of Results from the Monte Carlo Simulation with Average Values of 390 Diffuse Reflectance Spectra from 133 Test Persons[a]

	Monte Carlo Simulation Conditions ($-\log R_{diff}$)		Experimental Average Values with $\pm 2\sigma$ ($-\log R_{diff,exp}$)
$\tilde{\nu}$(cm^{-1})	Matched	Unmatched	
8000	0.57	0.785	0.71 ± 0.13
6350	1.06	1.39	1.21 ± 0.18
4400	1.60	1.96	1.91 ± 0.19

[a]The experimental values were calculated with reference to a white Spectralon reflectance standard.

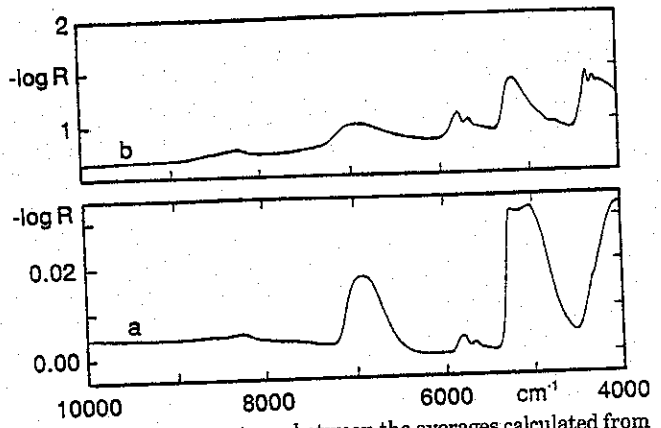

Fig. 8. Difference spectrum between the averages calculated from the spectra from 182 female and 199 male lips (trace a) and the diffuse reflectance spectrum of fatty minced beef (trace b).

In Fig. 7 an *in vivo* spectrum of the inner lip, as measured against a white standard (trace a), is shown. The achievable noise levels obtained from two consecutive spectra, each of mucous lip tissue, and a normally considered gray standard with reflectivity of 0.1 at 10,000 cm^{-1} are also presented (see traces b and c). Each noise level is wavelength dependent as a result of the spectrometer response. For illustration of the spectral energy distributions, single-beam spectra with a lip and a gray standard are also presented in Fig. 7 (see traces d and e, respectively). Spectral rms variations, particularly in the water OH-stretching overtone band below 7000 cm^{-1}, e.g., resulting from different contact pressure of the lip, are ~0.01 a.u. [$-\log R$ units interpreted as an absorbance unit (a.u.)] apart from baseline drifting with an offset in the same order.

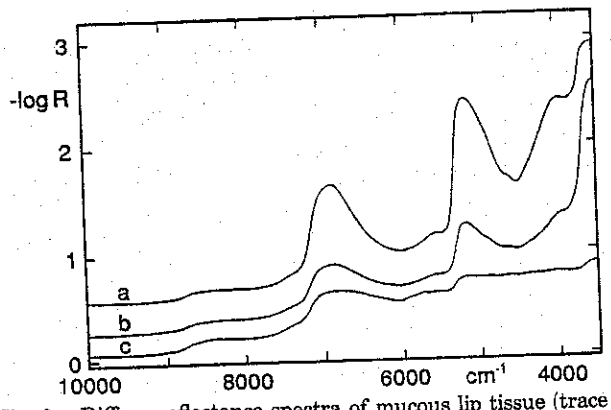

Fig. 9. Diffuse reflectance spectra of mucous lip tissue (trace a) compared with those of the upper tongue surface and of thumb skin from one person (traces b and c, respectively) (offset for clarity).

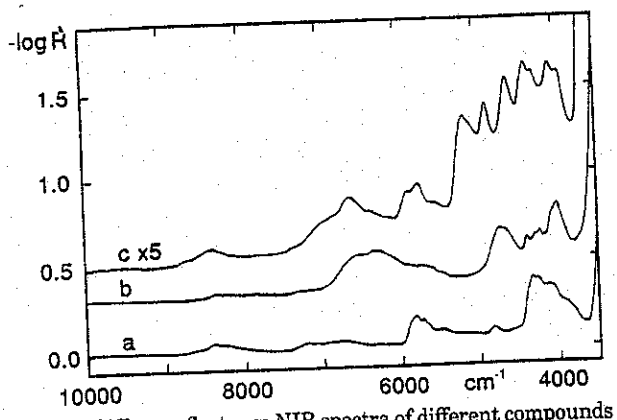

Fig. 10. Diffuse reflectance NIR spectra of different compounds of clinical interest: a, albumin as a model compound for protein; b, anhydrous crystalline glucose; c, cholesterol (offset for clarity).

The results from the Monte Carlo simulation can be compared with the experimental results from a clinical measurement campaign with 133 different test persons providing a total of 390 diffuse reflectance spectra of the lower inner lip (see Table 2). The average values are listed with twice the standard deviation derived from the spectrum population. The experimental results are in good agreement with the simulation results obtained for matched and unmatched boundary conditions confirming the optical parameters chosen for the Monte Carlo study. For the wave numbers at 8000 and 6350 cm^{-1} a better agreement is found than for 4400 cm^{-1}, which is possibly an effect of unsatisfactory extrapolation carried out for the optical parameters as described above. Another reason for the deviations in the simulated reflectance compared with the experimental values is certainly the layered structure of the mucous tissue, which has not been taken into account for modeling, so the differences may be partly a result of this simplification.

When the spectrum population from the test persons measured for evaluation of the possibility of a transcutaneous noninvasive glucose assay was studied in detail, we noticed some spectra that contain an absorption band doublet below 6000 cm^{-1} indicating subcutaneous fatty tissue being spectroscopically probed. In Fig. 8 the difference spectrum between the averages calculated from 182 female and 199 male lip spectra is shown. A diffuse reflectance spectrum of minced beef of considerable fat content is presented for illustration (trace b).

For completeness the spectra of some different types of human skin are presented in Fig. 9. A good optical contact to the lens can certainly be maintained for the mucous tissue of the inner lip, whereas, e.g., the upper rough surface of the tongue provides less contrast for the water absorption bands. A further decline exists for a skin sample with an established layer of stratum corneum as found for the thumb tip. The spectral examples for these species of skin tissue are that from a test of one male person.

Finally, an example related to the *in vivo* spectra is provided (see Fig. 10) where the spectra of albumin as a model compound for protein, anhydrous crystalline glucose, and cholesterol are shown, illustrating that the information content of the NIR spectral range is important, particularly for the *in vivo* spectroscopy of human tissue.

5. Conclusions

The accessory presented can be used to obtain *in vivo* diffuse reflectance spectra of high signal-to-noise ratios for various skin tissue materials. The main emphasis, however, was placed on the mucous tissue of the inner human lip. The achievable noise level could be further improved by use of radiation sources that provide greater spectral radiance in the wavelength range studied than the tungsten–halogen bulb used here as a standard spectrometer thermal source. The irradiance on the skin with the setup chosen is ~ 10 mW mm^{-2}. Here the use of lasers may be helpful; however, the maximum permissible radiation exposure levels are limited by damage effects to the tissue and must comply with safety standards.[42]

Multivariate spectrometry used for quantitative analysis is complicated by the variability of the measurement, i.e., mainly the result of differing lip position and contact pressure.[6,7] Furthermore the biological variation between individuals because of different tissue texture is, as expected, by far greater than for the measurements carried out during the test of one person, so multiperson calibrations for sensitive noninvasive blood glucose monitoring based on diffuse reflectance spectroscopy of tissue await further improvements in measurement reproducibility and calibration modeling when we take into account, e.g., individually different path lengths for the probing radiation.

Appendix A

The on-axis ellipsoidal mirror images the Lambertian radiating sample spot onto the detector. The effective magnification of this mirror influences the irradiation in the detection focal plane. For varying solid angles used for collecting the diffusely reflected radiation, this parameter is derived. The ellipsoidal mirror can be described by its ellipsoidal semiaxes a and b. As Korte[18] showed recently using $\gamma = a/b$ and $C = 2\gamma(\gamma^2 - 1)^{1/2}/(2\gamma^2 - 1)$, the magnification $U(\alpha)$ obtained by an infinitesimal mirror element is given by the ratio of its distances to the detection and sample focus. The angle α denotes the angle of a given ray with respect to the normal of the sampling focal plane of the ellipsoid. For small sample spots, compared with the radii of the ellipsoidal mirror, this magnification can be written[18]

$$U(\alpha) = (1 - C\cos\alpha)(1 - C^2)^{-1/2}. \qquad \text{(A1)}$$

Furthermore the so-called meridional magnification is relevant; it arises from the projection caused by differences between the surface normal of the sam-

pling and that of the detection plane compared with the corresponding infinitesimal mirror element radii[18]:

$$V(\alpha) = [(1 - C\cos\alpha)^2\cos\alpha]/[(1 - C^2)^{1/2}(C - \cos\alpha)]. \quad \text{(A2)}$$

A circular spot with radius r_0 is projected by such a mirror element onto an ellipse with its semiaxes $U(\alpha)r_0$ and $V(\alpha)r_0$, and the uniform irradiance in the detector plane is reduced by the factor $[U(\alpha)V(\alpha)]^{-1}$. We consider the case $V(\alpha) \le U(\alpha)$, which is valid for $\alpha \ge 30°$ given $\gamma = 2$; the other case can be handled accordingly.

The ellipse equation (see also Fig. 11) can be written

$$[r\cos\varphi/U(\alpha)]^2 + [r\sin\varphi/V(\alpha)]^2 = r_0^2, \quad \text{(A3)}$$

which provides us with the angle φ necessary for the following integration:

$$\varphi(r) = \arccos(\pm\{[1 - V^2(\alpha)r_0^2/r^2] / [1 - V^2(\alpha)/U^2(\alpha)]\}^{1/2}). \quad \text{(A4)}$$

The irradiance density function produced by an annular mirror element of constant angle α can be obtained by integration over the angle φ:

$$f(r, \alpha) = \begin{cases} 2\pi/[U(\alpha)V(\alpha)] & r \le V(\alpha)r_0 \\ \dfrac{4}{U(\alpha)V(\alpha)}\arccos\left[\dfrac{1 - V^2(\alpha)r_0^2/r^2}{1 - V^2(\alpha)/U^2(\alpha)}\right] & V(\alpha)r_0 < r \le U(\alpha)r_0. \\ 0 & U(\alpha)r_0 < r \end{cases} \quad \text{(A5)}$$

A plateau of constant irradiance is found within a circular spot of radius $V(\alpha)r_0$, whereas the density function decreases monotonically within the interval given in the second formula of Eq. (A5). For Lambertian radiation characteristics we obtain

$$f_{\text{tot}}(r, \alpha_0) = \int_{\alpha_0}^{90°} f(r, \alpha)2\pi\cos\alpha\sin\alpha\, d\alpha. \quad \text{(A6)}$$

This equation has been solved numerically. Further integration over the radial area, when we take into account this radial distribution, yields a cumulative distribution function of the radiant power dependent on r_{det}, the radius in the detection plane:

$$F_{\text{tot}}(r_{\text{det}}, \alpha_0) = \int_0^{r_{\text{det}}} f_{\text{tot}}(r, \alpha_0)2\pi r dr, \quad \text{(A7)}$$

which can be solved numerically to provide an effective value $V_{\text{eff}}(\alpha_0)$ of the linear magnification of the ellipsoidal mirror of given geometry, which reads for this derivation $V_{\text{eff}}(\alpha_0) = r_{\text{det}}/r_0$. Different quantiles of the radiant power of 75% and 90% were used to

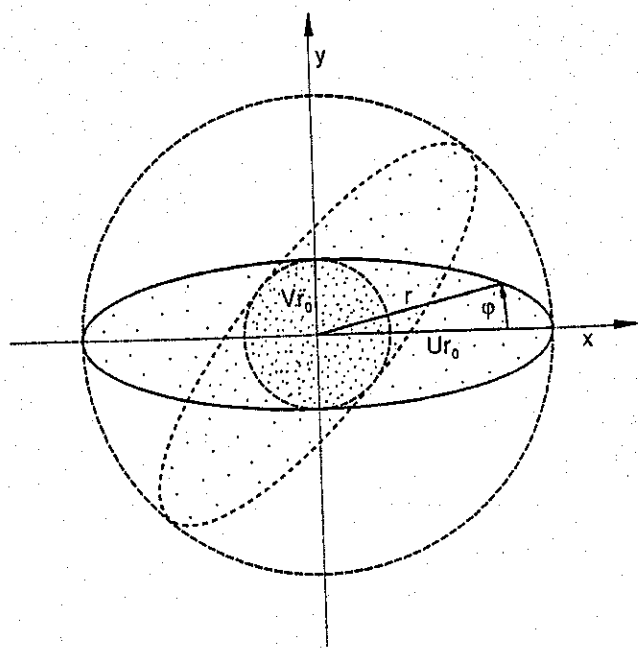

Fig. 11. Derivation of the α-dependent irradiance density function obtained in the detection focal plane of the on-axis ellipsoidal mirror. Two elliptical images are shown that are produced by different infinitesimal elements of a mirror ring with a constant half-open angle α (see also text).

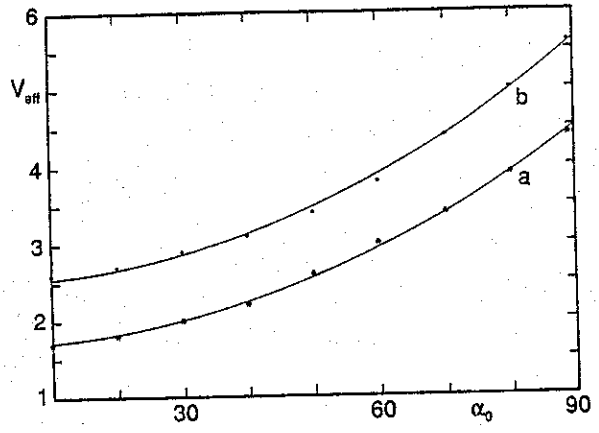

Fig. 12. Effective magnification of the ellipsoidal mirror depending on the maximum half-angle α_0 defining the illumination cone. The parameters are different percentage quantiles of the radial distribution of the radiant power in the detector plane (the solid curves are the result of a polynomial fit; for the results see text): a, 75% quantile; b, 90% quantile.

evaluate the α_0-dependent parameter r_{det}. The functional dependence of the effective magnification is illustrated in Fig. 12. A polynomial fit was derived for the quantiles chosen with $V_{eff}(\alpha_0) = K_0 + K_1\alpha_0^2$ with α_0 provided in degrees. The results are for 75%, $K_0 = 1.68$, $K_1 = 3.47 \times 10^{-4}$, and for 90%, $K_0 = 2.51$, $K_1 = 3.85 \times 10^{-4}$. The effective magnification for the 75% quantiles was considered for the study of the optimum collection cone described in Section 2.

Financial support by the Deutsche Forschungsgemeinschaft, the Ministerium für Wissenschaft und Forschung des Landes Nordrhein-Westfalen and the Bundesminister für Forschung und Technologie is gratefully acknowledged. The authors thank H. Otto (Pathologisches Institut, Dortmund) for the lip tissue samples studied by light microscopy.

References

1. J. L. Bulnois, "Photophysical processes in recent medical laser developments: a review," Lasers Med. Sci. **1,** 47–66 (1986).
2. J. A. Parrish, "New concepts in therapeutic photomedicine: photochemistry, optical targeting and the therapeutic window," J. Invest. Dermatol. **77,** 45–50 (1981).
3. P. Rolfe, ed., *Non-Invasive Physiological Measurements* (Academic, London, 1979), Vol. 1; (1983), Vol. 2.
4. M. Cope and D. T. Delpy, "System for long-term measurement of cerebral blood and tissue oxygenation on newborn infants by near infrared transillumination," Med. Biol. Eng. Comput. **26,** 289–294 (1988).
5. H. M. Heise, R. Marbach, T. Koschinsky, and F. A. Gries, "Multivariate determination of blood substrates in human plasma by FT-NIR spectroscopy," in *Proceedings of the Eighth International Conference on Fourier Transform Spectroscopy,* H. M. Heise, E. H. Korte, and H. W. Siesler, eds., Proc. Soc. Photo-Opt. Instrum. Eng. **1575,** 507–508 (1992).
6. R. Marbach, *Meßverfahren zur IR-spektrometrischen Blutglucosebestimmung,* Fortschr. Ber. VDI Ser. 8 (VDI-Verlag, Düsseldorf, 1993), Vol. 346.
7. R. Marbach, T. Koschinsky, F. A. Gries, and H. M. Heise, "Noninvasive blood glucose assay by near-infrared diffuse reflectance spectroscopy of the human inner lip," Appl. Spectrosc. **47,** 875–881 (1993).
8. N. Kaiser, "Methods for determining the contents of metabolic products in the blood," U.S. patent 4,169,676 (2 Oct. 1979); N. Kaiser, "Laser absorption spectroscopy with an ATR prism," IEEE Trans. Biomed. Eng. **BME-26,** 597–600 (1979).
9. K. Kajiwara, T. Uemura, H. Kishikawa, K. Nishida, Y. Hashiguchi, M. Uehara, M. Sakakida, K. Ichinose, and M. Shichiri, "Noninvasive measurement of blood glucose concentrations by analysing Fourier transform infra-red absorbance spectra through oral mucosa," Med. Biol. Eng. Comput. **31,** S17–S22 (1993).
10. W. Richter and W. Erb, "Accurate diffuse reflection measurements in the infrared spectral range," Appl. Opt. **26,** 4620–4624 (1987).
11. D. Sheffer, U. P. Oppenheim, D. Clement, and A. D. Devir, "Absolute reflectometer for the 0.8–2.5-μm region," Appl. Opt. **26,** 583–586 (1987).
12. D. Sheffer, U. P. Oppenheim, and A. D. Devir, "Absolute reflectometer for the mid-infrared region," Appl. Opt. **29,** 129–132 (1990).
13. R. Hogue, "Praying Mantis' diffuse reflectance accessory for UV-Vis-NIR spectroscopy," Fresenius Z. Anal. Chem. **339,** 68–69 (1991).
14. A. Otto, *Infrarotspektroskopie mit diffus reflektierter Strahlung: In-situ Messungen an schwach streuenden Proben,* Fortschr. Ber. VDI Ser. 8 (VDI-Verlag, Düsseldorf, 1987), Vol. 146.
15. S. T. Dunn, J. C. Richmond, and J. A. Wiebelt, "Ellipsoidal mirror reflectometer," J. Res. Natl. Bur. Stand. **70C,** 75–88 (1966).
16. M. P. Fuller and P. R. Griffiths, "Diffuse reflectance measurements by infrared Fourier transform spectroscopy," Anal. Chem. **50,** 1906–1910 (1978).
17. H. Maulhardt and D. Kunath, "Diffuse reflectance spectroscopy in the infrared," Talanta **29,** 237–241 (1982).
18. E. H. Korte, "Figures of merit for a diffuse reflectance accessory using an on-axis ellipsoidal collecting mirror," Appl. Spectrosc. **42,** 428–433 (1988).
19. E. H. Korte and A. Otto, "Infrared diffuse reflectance accessory for local analysis on bulky samples," Appl. Spectrosc. **42,** 38–43 (1988).
20. T. Hirschfeld, "Optimization of diffuse reflectance infrared spectroscopy accessories," Appl. Spectrosc. **40,** 1082–1085 (1986).
21. D. W. Sting, "Multiple internal reflection cell optical system for use in infrared spectrophotometry of liquids and fluidized samples," U.S. patent 4,595,833 (17 June 1986).
22. I. H. Malitson, "A redetermination of some optical properties of calcium fluoride," Appl. Opt. **2,** 1103–1107 (1963).
23. W. J. Smith, *Modern Optical Engineering* (McGraw-Hill, New York, 1966), p. 233.
24. G. Kortüm, *Reflexionsspektroskopie* (Springer-Verlag, Berlin, 1969), p. 15.
25. B. C. Wilson and S. L. Jacques, "Optical reflectance and transmittance of tissues: principles and applications," IEEE J. Quantum Electron. **26,** 2186–2199 (1990).
26. S. T. Flock, M. S. Patterson, B. C. Wilson, and D. R. Wyman, "Monte Carlo modeling of light propagation in highly scattering tissues. I: Model predictions and comparison with diffusion theory," IEEE Trans. Biomed. Eng. **36,** 1162–1168 (1989).
27. M. J. C. van Gemert, S. L. Jaques, H. J. C. M. Sterenborg, and W. M. Star, "Skin optics," IEEE Trans. Biomed. Eng. **36,** 1146–1154 (1989).
28. W. F. Cheong, S. A. Prahl, and A. J. Welch, "A review of the optical properties of biological tissues," IEEE J. Quantum Electron. **26,** 2166–2185 (1990).
29. D. R. Wyman, M. S. Patterson, and B. C. Wilson, "Similarity relations for the interaction parameters in radiation transport," Appl. Opt. **28,** 5243–5249 (1989).
30. S. T. Flock, B. C. Wilson, and M. S. Patterson, "Total attenuation coefficients and scattering phase functions of tissues and phantom materials at 633 nm," Med. Phys. **14,** 835–841 (1987).
31. S. L. Jacques, C. A. Alter, and S. A. Prahl, "Angular dependence of He–Ne laser light scattering by human dermis," Lasers Life Sci. **1,** 309–333 (1987).
32. R. Marchesini, A. Bertoni, S. Andreola, E. Melloni, and A. E. Sichirollo, "Extinction and absorption coefficients and scattering phase functions of human tissues *in vitro,*" Appl. Opt. **28,** 2318–2324 (1989).
33. L. G. Henyey and J. L. Greenstein, "Diffuse radiation in the galaxy," Astrophys. J. **93,** 70–83 (1941).
34. F. P. Bolin, L. E. Preuss, R. C. Taylor, and R. J. Ference, "Refractive index of some mammalian tissues using a fiber optic cladding method," Appl. Opt. **28,** 2297–2303 (1989).
35. G. M. Hale and M. R. Querry, "Optical constants of water in the 200-nm to 200-μm wavelength region," Appl. Opt. **12,** 555–563 (1973).
36. P. Parsa, S. L. Jacques, and N. S. Nishioka, "Optical properties of rat liver between 350 and 2200 nm," Appl. Opt. **28,** 2325–2330 (1989).
37. J. D. Hardy, H. T. Hammell, and D. Murgatroyd, "Spectral

transmittance and reflectance of excised human skin," J. Appl. Physiol. **9**, 257–264 (1956).
38. D. J. Maitland, J. T. Walsh, Jr., and J. B. Prystowsky, "Optical properties of human gallbladder tissue and bile," Appl. Opt. **32**, 586–591 (1993).
39. R. R. Meier, J.-S. Lee, and D. E. Anderson, "Atmospheric scattering of middle UV radiation from an internal source," Appl. Opt. **17**, 3216–3225 (1978).
40. R. A. J. Groenhuis, H. A. Ferwerda, and J. J. ten Bosch, "Scattering and absorption of turbid materials determined from reflection measurements. 1: Theory," Appl. Opt. **22**, 2456–2462 (1983).
41. Catalog data from Labsphere, North Sutton, N.H.
42. D. H. Sliney, "Radiation safety. The maximum permissible exposure levels: our knowledge of the hazards," Opt. Laser Technol. **21**, 235–240 (1989).